Optics Letters

Fabrication and characterization of super-polished wedged borosilicate nano-cells

T. Peyrot,[1] Ch. Beurthe,[1] S. Coumar,[1] M. Roulliay,[1] K. Perronet,[1] P. Bonnay,[2] C. S. Adams,[3] A. Browaeys,[1] and Y. R. P. Sortais[1,*]

[1]Laboratoire Charles Fabry, Institut d'Optique Graduate School, CNRS, Université Paris-Saclay, 91127 Palaiseau Cedex, France
[2]Laboratoire GEPI, CNRS, Univ. Paris-Diderot, Observatoire de Paris, 11 avenue de l'Observatoire, 75014 Paris, France
[3]Department of Physics, Rochester Building, Durham University, South Road, Durham DH1 3LE, UK
*Corresponding author: yvan.sortais@institutoptique.fr

Received 10 January 2019; revised 27 February 2019; accepted 1 March 2019; posted 4 March 2019 (Doc. ID 357428); published 5 April 2019

We report on the fabrication of an all-glass vapor cell with a thickness varying linearly between (exactly) 0 and ∼1 μm. The cell is made in Borofloat glass that allows state-of-the-art super polish roughness, a full optical bonding assembling and easy filling with alkali vapors. We detail the challenging manufacture steps and present experimental spectra resulting from fluorescence and transmission spectroscopy of the cesium D1 line. The very small surface roughness of 1 Å rms is promising to investigate the atom-surface interaction or to minimize parasite stray light.

https://doi.org/10.1364/OL.44.001940

Miniaturization of devices based on atomic vapor has set the stage for the development of various compact light–matter interfaces [1,2]. However, to reach high precision performances required to be used as atomic sensors [3,4], integrated optical chips immersed in alkali vapors demand meticulous characterization. In this perspective, vapor nano-systems [5–7] have recently been used to clarify fundamental problems in optics such as the role of dipole interactions in resonant light scattering [7,8], to control the coherent excitation of Rydberg atoms [9], or to evidence the non-local response of an atomic gas [10]. Another issue inherent to the system size reduction is the growing influence of the atom-surface interaction, which triggered the development of new glass nano-cells [11–13]. In addition, by combining short repulsive and long attractive potential, the possibility to trap atoms in bound states has theoretically been predicted [14], and this ability could make way for hybrid nanoscale atom-surface meta-materials [15].

In this Letter, we report on the fabrication of a glue-free all-glass nano-cell with a thickness varying linearly between (exactly) 0 and ∼1 μm, and with a surface roughness of 1 Å rms. Filled with cesium (Cs), the cell was initially built for the interrogation of small atomic vapor layers of alkali and to investigate the hypothetical existence of an atom-surface bound state that would depend on the surface corrugation [16]. Developing surfaces with ultra-low surface roughness is also an asset to reduce parasite scattering, limiting the signal-to-noise ratio of light–matter interaction with nanometric atomic ensembles. Besides, the super-polish surfaces presented here can be ideal candidates for the fabrication of glass micro-cavities for quantum electrodynamics experiments [17]. Therefore, the techniques that we present may have a large panel of applications and find audience in diverse domains such as surface science optics and atomic physics. We will first describe the cell fabrication process and how we filled it with Cs. We subsequently present the methods to check the requirements in terms of surface roughness and cell thickness. Finally, we bring forward promising examples of spectra in transmission and off-axis fluorescence of the Cs D1 line.

The cell was fabricated at Laboratoire Charles Fabry of Institut d'Optique (Palaiseau, France) and filled with a Cs vapor at the Laboratoire GEPI of Observatoire de Paris (Paris, France). It is made of four parts that are assembled by optical contact bonding leading to a monolithic ensemble [see Fig. 1(a)]. Using the same material for all parts avoids differential thermal expansion that could damage the optical bonding. Borofloat glass has been chosen for its good optical properties in the visible and near-infrared spectrum, and facility to be super-polished in comparison to other materials used in previous cells (sapphire for instance). This glass was also chosen to facilitate the sealing to the Pyrex side arm that will contain the Cs reservoir, as the thermal expansion coefficients and the softening temperatures of both glasses are similar. However, unlike sapphire, and similar to fused silica, it reacts with alkali at temperatures exceeding ∼200°C. The central part (A) [see Fig. 1(b)] is machined using boring-bits so as to let a 6 mm external diameter, 4 mm internal diameter, and 25 mm long tube protrude from the front face to allow for connection to a Pyrex loading manifold containing the Cs reservoir. Glass is then removed from the inside of part (A) using milling-bits. In this hollow piece, a thick plate (B), carefully angled on one side, is introduced. The cell is closed by two thick plates (C_L) and (C_R) wedged by 1° to dismiss unwanted reflections.

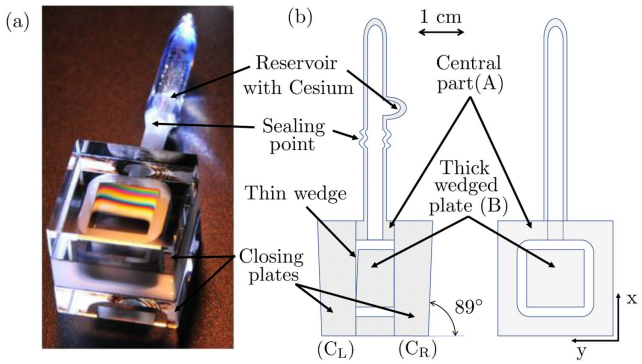

Fig. 1. (a) Photograph of the cell. The white light color fringes reflect the thickness variations in the wedge of the nano-cell. (b) Schematic of the cell.

Plate (B) is optically contacted on one side on plate (C_R). On the other side, the gap formed by the angle between plate (B) and plate (C_L) forms the nano-enclosure and, therefore, its realization is crucial. The two main manufacturing difficulties that we will detail are (1) the control of the nano-gap thickness and (2) the polishing of the different surfaces to reach excellent surface roughness.

The thin wedge of plate (B) is realized by polishing iterations and controls of the wedge thickness and flatness between two polishing steps. This is done interferometrically, using a He–Ne laser and a Fizeau interferometer. The wedge is realized such that four fringes appear in the interferogram, parallel to the y axis (see Fig. 1) with equal interfringe spacing. This corresponds to a thickness variation of 1.2 μm. In addition, the absolute thickness is controlled such that, along its thickest edge, the plate thickness exceeds the thickness of plate (A) by ∼300 nm [see Fig. 2(a)], forming a ridge that will eventually be removed. This is controlled mechanically, using an electronic depth gauge with a resolution of 100 nm. Parts A and B are then optically contacted on a parallel plate (P_1) and polished simultaneously so as to remove the 300 nm thick ridge and bring parts (A) and (B) to equal height for closing purpose. This height equalization is controlled interferometrically using a flat etalon (P_2), as shown in Fig. 2. This procedure ensures that final assembly brings the closing plate (C_L) in optical contact with both parts (A) and (B). Therefore, the wedge thickness varies between (exactly) 0 and about 900 nm.

To realize surfaces with very low roughness such as those inside the thin wedge, we first grind them finely using alumina

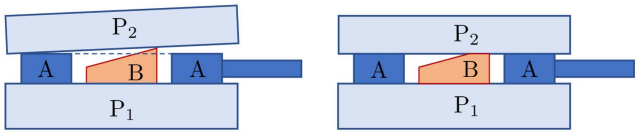

Fig. 2. Procedure to realize a thin wedge with thickness varying between (exactly) 0 and 900 nm. Parts (A) and (B) are optically contacted on a parallel plate (P_1). Left: the thickness of part (B) first exceeds that of part (A) by 300 nm. Therefore, flat etalon P_2 on the ridge of part (B), leading to interference fringes [between part (A) and the flat etalon] with different white light colors on each side of the ridge. Right: after flattening the ridge and equalizing the heights of part (A) and (B), the flat etalon sits equally on parts (A) and (B), leading to equal color fringes.

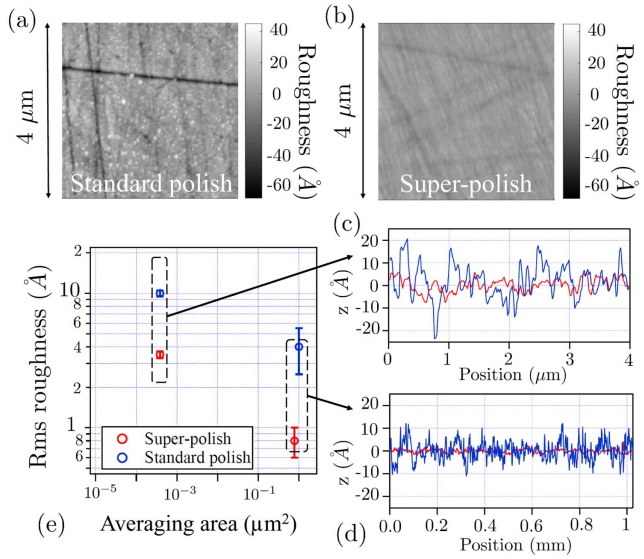

Fig. 3. (Top): AFM imaging of (a) a standard polish and (b) a super-polished surface of our cell. (Bottom): roughness profiles acquired with (c) the AFM and a spatial resolution of 20 nm and (d) the optical heterodyne profiler (spatial resolution: 1 μm). Red (blue) traces correspond, respectively, to the super-polish (standard polish) surfaces. (e) RMS roughness versus averaging area.

abrasives and a brass grinding wheel. The surfaces are then manually polished on a pitched wheel using an aqueous solution of rare earth oxide abrasives with a fine particle size (<1 μm). The final polish is performed with an increasingly diluted solution, leading to a super-polish with a surface roughness of 1 Å rms or less. To the best of our knowledge, compared to other polishing methods, this procedure leads to state-of-the-art roughness on borosilicate glass [18–25]. Figure 3(d) shows a typical roughness profile, measured using an optical heterodyne profiler (ZYGO 5500) with a sensitivity of 0.2 Å rms [26]. The spatial resolution of the profiler is 1 μm, on the order of the distance travelled by the atomic dipoles of the vapor before they reach a steady state (limited by collisions inside the gas or radiative decay). To investigate atom-surface interactions over shorter travelling distances, and account for the transient response of the vapor to finer details of the surface [10], we characterize the surface on a smaller scale. To do so, we acquired images of the super-polished surfaces using an atomic force microscope (AFM) in a tapping mode, equipped with a silicon tip (n-type) [27]. The spatial resolution of the AFM imaging is given by the radius of the tip, typically 10 nm or less. Typical images and roughness profiles acquired with the AFM are shown in Figs. 3(a)–3(c) for a super-polish and a standard polish. The standard polish is obtained by using rougher abrasives and stopping the polishing procedure before the above-mentioned final dilution step. Figure 3(e) compares the results obtained for surfaces with a super-polish and a standard polish. The roughness is lower for a super-polish than a standard polish, as expected, and it decreases for lesser spatial resolutions, as surface height fluctuations are better averaged [28].

All parts of the cell are cleaned with alcohol prior to final assembly by optical contact bonding (no glue is used). The

bonding of two surfaces is done at room temperature. It relies on the presence of hydroxyl molecules, which are bonded to the silicon atoms of the glass and bring the two surfaces together by hydrogen bonding, mediated by the presence of water molecules [13,29,30]. The bonding is obtained by pressing lightly onto the parts to be bonded until white light color fringes disappear and are replaced by a uniform dark fringe where the two parts are in contact. The only requirements are the absence of dust and the complementarity of the two surfaces to be bonded: in our case, we found that a flatness difference of 30 nm rms or less was sufficient to achieve a stress-resistant and vacuum-tight optical bonding.

Once the cell is assembled we connected it to a turbomolecular pumping stage via a Pyrex loading manifold, and baked the cell-manifold assembly at 350°C–400°C for four days while pumping. Although the pressure inside the cell cannot be evaluated precisely [31], this procedure proved to be necessary both to get rid of water vapor and residual contaminants inside the cell prior to filling with Cs vapor and to reinforce the optical bonding. Cs was then transferred, using a low temperature flame, from a Cs ampoule with a breakable seal to the cell reservoir. We note that the optical bonding resisted and was actually reinforced by the baking cycles. It also resisted subsequent cycles between room temperature and 200°C, allowing for spectroscopic studies with variable atomic density.

We now provide more information about our *in situ* measurement of the wedge thickness. We access the local absolute thickness $L(x,y)$ using the interferometric technique described in Ref. [32]. The reflected intensity R_w resulting from the interference on the thin wedge [see Fig. 4(a)] tells about the local thickness: by scanning the laser position along the x axis of the cell, from the optical contact to the thickest part of the wedge, we record on a power meter the interferometric profile shown in Fig. 4(b). The optical contact is reached for $x \leq x_0$. For $x > x_0$ and a given value of y, the data are very well fitted by the Fabry–Perot model:

$$R_w(x) \propto \frac{F \sin^2(\phi(x)/2)}{1 + F \sin^2(\phi(x)/2)}, \tag{1}$$

with $F = 4r^2/(1-r^2)^2 = (2\mathcal{F}/\pi)^2$ ($\mathcal{F}$ is the finesse of the wedge etalon), $r = (n_g - n)/(n_g + n)$, the reflectivity (in field amplitude) of the glass-to-vapor interface; n_g being the glass refractive index, n, the refractive index of the vapor; and $\phi(x) = 4\pi L(x)/\lambda$, the cumulative phase over one round-trip of the laser inside the wedge. Here we assume that the wedge thickness varies linearly with x for $x > x_0$ and, therefore, the only free parameter of the fit is the wedge angle, $\alpha(y) = L(x,y)/(x - x_0)$. In addition, we perform this interferometric mapping of the thickness at very low vapor pressure and with a laser light far detuned from the atomic resonances. The vapor index n, therefore, can be assimilated to unity. Figure 4(c) shows a 2D map of $L(x,y)$. The uncertainty on each point is ± 5 nm, limited by the finite size of the laser beam (waist radius $w_0 \simeq 40$ μm).

Finally, we present examples of spectroscopic data obtained with the cell described above. The cell was enclosed in an oven with small apertures to let a laser beam propagate through the wedge and to collect the fluorescence light at 90° from the laser beam. With this setup, we acquired the absorption and fluorescence spectra shown in Fig. 5. These spectra were obtained

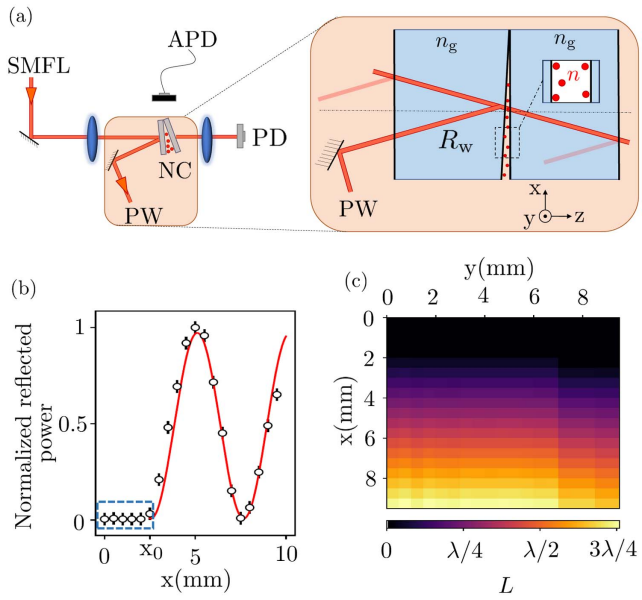

Fig. 4. (a) Schematic of the experiment. SMFL, single-mode fiber laser; PD, Si photodiode; APD, avalanche photodiode for fluorescence measurements; NC, nano-cell, PW, power meter. (b) Reflected interference signal $R_w(x)$ (normalized to the signal obtained at a bright fringe). Black circles, data acquired for $y = 5$ mm; solid red line, fit by the Fabry–Perot model. For $x < x_0$ (dashed blue rectangle), the wedge thickness is exactly zero, since parts (B) and (C_L) are optically bonded [see Fig. 1(b)]. (c) 2D mapping of the wedge thickness (resolution along x and y: 0.5 mm).

by scanning the frequency of a laser diode around the D1 line of Cs at $\lambda = 894$ nm. In practice, one should pay attention to maintain the temperature of the wedge 30°C higher that the temperature of the Cs reservoir to avoid Cs to condense on the wedge when the temperature is ramped down below the melting point. The spectra of Fig. 5 were obtained at a cell temperature of 170°C (temperature of the reservoir,

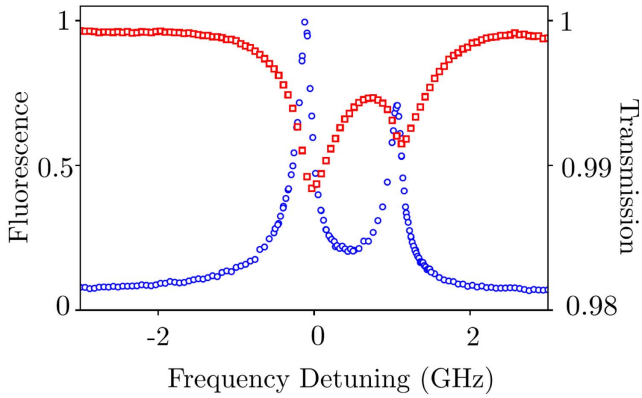

Fig. 5. Spectra of the D1 line of Cs acquired using the nano-cell described in the main text, heated at 170 ± 5°C. Cell thickness, $L = 95 \pm 5$ nm; in blue circles (red squares), normalized fluorescence spectrum collected at 90° from laser propagation (absorption spectrum). Horizontal axis: laser frequency detuning with respect to the $F = 4 \rightarrow F' = 3$ hyperfine transition of the $6S_{1/2}$ ground state. The peak centered at 1 GHz corresponds to the $F = 4 \rightarrow F' = 4$ transition. The data are binned 10 times by steps of 2 MHz.

corresponding to an atomic density $N = 5.6 \times 10^{14}$ cm^{-3}). The laser was focused onto the thin wedge at a point where the local thickness is $L = 95$ nm $\simeq \lambda/10$. The laser power was ~1 μW, and the laser spot at $1/e^2$ radius was 40 μm. The transmitted light was collected onto a standard Si photodiode. We simultaneously acquired the fluorescence spectrum using a fibered avalanche photodiode in a photon counting mode. The overall detection efficiency was $\sim 1.5 \times 10^{-3}$, accounting for the solid angle collection efficiency (7.5×10^{-3}), the fiber coupling (50%), and the photodiode quantum efficiency (40%). The possibility to acquire data on a zero background may improve the signal-to-noise ratio in comparison with transmission spectra. Both spectra in fluorescence and transmission exhibit a narrow lineshape (smaller than Doppler width), characteristic of the Dicke narrowing observed in nano-cells [33].

In conclusion, we have built a new generation of nano-cells that presents many advantages. The cell parts are made of Borofloat glass that allows a very good polishing and, therefore, a very small surface roughness. It also allows us to connect all parts of the cell with optical bonding, resulting in a monolithic cell that does not use glue. Therefore, it avoids any degassing issues for future spectroscopic studies. For the surfaces in contact with the atoms in the nano-wedge, a super-polish is obtained, and the surface roughness is less than 1 Å rms. The wedge has been realized and characterized using interferometric techniques and the thickness of the cell ranges from exactly zero (optical contact) to 900 nm. Few-nanometer thick atomic vapors have never been probed due to the way nano-cells were closed prior to this Letter. The type of cells presented here open up access for the exploration of new mesoscopic systems. The spectra measured using these cells are promising for future investigation of atom-surface interactions. Our fabrication technique, in principle, allows us to cover the cell surfaces with a dielectric layer to increase the reflectivity and, hence, the dipole-dipole collective effects. The fabrication, theoretically, is not restricted to glass, and testing it with other materials could provide more data on unknown atom-surface potentials. Finally, such cells could be used as in Ref. [34] to perform molecular spectroscopy with various confinement depths.

Funding. Direction Générale de l'Armement (DGA) (2015600028); Engineering and Physical Sciences Research Council (EPSRC) (EP/R002061/1); Centre National de la Recherche Scientifique (CNRS); Durham University.

Acknowledgment. The authors thank T. Pfau for fruitful discussions and J. Moreau for helping us analyze the AFM images. T. Peyrot is supported by the DGA-DSTL fellowship 2015600028.

REFERENCES AND NOTES

1. W. Wasilewski, K. Jensen, H. Krauter, J. J. Renema, M. V. Balabas, and E. S. Polzik, Phys. Rev. Lett. **104**, 133601 (2010).
2. T. Petelski, M. Fattori, G. Lamporesi, J. Stuhler, and G. M. Tino, Eur. Phys. J. D **22**, 279 (2003).
3. S. Knappe, P. D. D. Schwindt, V. Shah, L. Hollberg, J. Kitching, L. Liew, and J. Moreland, Opt. Express **13**, 1249 (2005).
4. H. Fan, S. Kumar, J. Sheng, J. P. Shaffer, C. L. Holloway, and J. A. Gordon, Phys. Rev. A **4**, 044015 (2015).
5. D. Sarkisyan, T. Varzhapetyan, A. Sarkisyan, Y. Malakyan, A. Papoyan, A. Lezama, D. Bloch, and M. Ducloy, Phys. Rev. A **69**, 065802 (2004).
6. D. Sarkisyan, D. Bloch, A. Papoyan, and M. Ducloy, Opt. Commun. **200**, 201 (2001).
7. R. Ritter, N. Gruhler, H. Dobbertin, H. Kübler, S. Scheel, W. Pernice, T. Pfau, and R. Löw, Phys. Rev. X. **8**, 021032 (2018).
8. T. Peyrot, Y. R. P. Sortais, A. Browaeys, A. Sargsyan, D. Sarkisyan, J. Keaveney, I. G. Hughes, and C. S. Adams, Phys. Rev. Lett. **120**, 243401 (2018).
9. H. Kübler, J. P. Shaffer, T. Baluktsian, R. Löw, and T. Pfau, Nat. Photonics **4**, 112 (2010).
10. T. Peyrot, Y. R. P. Sortais, A. Browaeys, A. Sargsyan, J. Keaveney, I. G. Hughes, and C. S. Adams, Phys. Rev. Lett. **122**, 113401 (2019).
11. T. Baluktsian, C. Urban, T. Bublat, H. Giessen, R. Löw, and T. Pfau, Opt. Lett. **35**, 1950 (2010).
12. K. A. Whittaker, J. Keaveney, I. G. Hughes, A. Sargysyan, D. Sarkisyan, B. Gmeiner, V. Sandoghdar, and C. S. Adams, J. Phys. Conf. Ser. **635**, 122006 (2015).
13. K. A. Whittaker, "Construction and characterisation of ultra-thin alkali-metal vapour cells," Ph.D. dissertation (University of Durham, 2017).
14. E. G. Lima, M. Chevrollier, O. D. Lorenzo, P. C. Segundo, and M. Oriá, Phys. Rev. A. **62**, 013410 (2000).
15. K. A. Whittaker, J. Keaveney, I. G. Hughes, A. Sargsyan, D. Sarkisyan, and C. S. Adams, Phys. Rev. Lett. **112**, 253201 (2014).
16. M. C. Vargas and W. L. Mochán, Surf. Sci. **409**, 130 (1998).
17. A. Roy and D. Barrett, App. Phys. Lett. **99**, 171112 (2011).
18. A. J. Leistner, E. G. Thwaite, F. Lesha, and J. M. Bennett, Appl. Opt. **31**, 1472 (1992).
19. J. M. Bennett, J. J. Shaffer, Y. Shibano, and Y. Namba, Appl. Opt. **26**, 696 (1987).
20. Y. Li, J. Hou, Q. Xu, J. Wang, W. Yang, and Y. Guo, Opt. Express **16**, 10285 (2008).
21. B. E. Gillman and S. D. Jacobs, Appl. Opt. **37**, 3498 (1998).
22. F. Frost, B. Ziberi, A. Schindler, and B. Rauschenbach, Appl. Phys. A **91**, 551 (2008).
23. J. Zhang, B. Wang, and S. Dong, Front. Electr. Electron. Eng. China **3**, 480 (2008).
24. V. Jain, J. Mater. Process. Technol. **209**, 6022 (2009).
25. M. Kanaokaa, C. Liu, K. Nomura, M. Ando, H. Takino, and Y. Fukuda, J. Vac. Sci. Technol. B **25**, 2110 (2007).
26. G. E. Sommargren, Appl. Opt. **20**, 610 (1981).
27. Keysight Technologies, "AFM model: 5500 AFM."
28. The fluctuations average differently for a super-polish and a standard polish. This may be attributed to the spatial frequency distributions of surface height fluctuations being intrinsically different.
29. J. A. Dziuban, *Bonding in Microsystem Technology* (Springer, 2006).
30. N. Cocheteau, "Caractérisation et modélisation d'une adhérence moléculaire renforcée," Ph.D. thesis (Université d'Aix-Marseille, 2014).
31. At the end of the pumping procedure, we measured a pressure of 8×10^{-9} mbar at the pumping stage and at room temperature. The pressure inside the cell is certainly higher, due to the limited conductance of the Pyrex loading manifold.
32. E. Jahier, J. G. Ena, P. Jacquier, M. Lintz, A. V. Papoyan, and M. A. Bouchiat, Appl. Phys. B **71**, 561 (2000).
33. G. Dutier, A. Yarovitski, S. Saltiel, A. Papoyan, D. Sarkisyan, D. Bloch, and M. Ducloy, Eur. Lett. **63**, 35 (2003).
34. B. Gmeiner, A. Maser, T. Utikal, S. Götzinger, and V. Sandoghdar, Phys. Chem. Chem. Phys **18**, 19588 (2016).